Spectroscopic study of globular clusters in the halo of M31 with the Xinglong 2.16 m telescope II: dynamics, metallicity and age *

Zhou Fan[1], Ya-Fang Huang[1,2], Jin-Zeng Li[1], Xu Zhou[1], Jun Ma[1] and Yong-Heng Zhao[1]

[1] Key Laboratory of Optical Astronomy, National Astronomical Observatories, Chinese Academy of Sciences, Beijing 100012, China; *zfan@bao.ac.cn*
[2] Graduate University of Chinese Academy of Sciences, Beijing 100049, China

Abstract In Paper I, we performed spectroscopic observations on 11 confirmed globular clusters (GCs) in M31 with the Xinglong 2.16 m telescope. We mainly focused on the fitting method and the metallicity gradient for the M31 GC sample. Here, we analyze and further discuss the dynamics, metallicity and age, and their distributions, as well as the relationships between these parameters. In our work, eight more confirmed GCs in the halo of M31 were observed, most of which lack previous spectroscopic information. These star clusters are located far from the galactic center at a projected radius of ~ 14 to ~ 117 kpc, which is more spatially extended than that in the previous work. Firstly, we measured the Lick absorption-line indices and the radial velocities. Then the ages and metallicity values of $[\mathrm{Fe/H}]$ and $[\alpha/\mathrm{Fe}]$ were fitted by comparing the observed spectral feature indices and the Single Stellar Population model of Thomas et al. in the Cassisi and Padova stellar evolutionary tracks, respectively. Our results show that most of the star clusters in our sample are older than 10 Gyr except B290, which is ~ 5.5 Gyr, and most of them are metal-poor with metallicity $[\mathrm{Fe/H}] < -1$, suggesting that these clusters were born at the early stage of the galaxy's formation. We find that the metallicity gradient for the outer halo clusters with $r_{\mathrm{p}} > 25$ kpc may have an insignificant slope of -0.005 ± 0.005 dex kpc^{-1} and if the outliers G001 and H11 are excluded, the slope does not change significantly, with a value of -0.002 ± 0.003 dex kpc^{-1}. We also find that the metallicity is not a function of age for the GCs with age < 7 Gyr, but for the old GCs with age > 7 Gyr, there seems to be a trend that the older ones have lower metallicity. Additionally, we plot metallicity distributions with the largest sample of M31 GCs so far and show the bimodality is not significant, and the number of metal-poor and metal-rich groups becomes comparable. The spatial distributions show that the metal-rich group is more centrally concentrated but the metal-poor group occupies a more extended halo. In addition, the young population is centrally concentrated but the old population is more spatially extended towards the outer halo.

Key words: galaxies: individual (M31) — galaxies: star clusters — globular clusters: general — star clusters: general

1 INTRODUCTION

One way to better understand the formation and evolution of galaxies is through detailed studies of globular clusters (GCs), which are often considered to be the fossils of galactic formation and evolutionary processes, since they formed in the early stages of their host galaxies' life cycles (Barmby et al. 2000). GCs are densely packed, very luminous, and usually contain several thousand to approximately one million stars. Therefore, they can be detected from great distances and are suitable as probes for studying the properties of extragalactic systems. Since the halo globular clusters (HGCs) are located far away from the galactic center, they are very important and can be used to study the dark matter distribution of the galaxy. In addition, as the HGCs are far from the center of the galaxy, the background of a galaxy becomes much dimmer, which makes the observations much easier compared to observing disk GCs in the projected direction of galaxies.

As the nearest ($\sim$ 780 kpc) large spiral galaxy in our Local Group, M31 (Andromeda) contains many GCs, with the number ranging from 460 ± 70 (Barmby & Huchra 2001) to $\sim$530 (Perina et al. 2010), which is an ideal laboratory for us to study the nature of HGCs. Many new M31 HGCs have been discovered in recent years, and they are an important tool to study the formation history of M31 and its dark matter content. Huxor et al. (2004) discovered nine previously unknown HGCs of M31 using the INT survey. Subsequently, Huxor et al. (2005) found three new, extended GCs in the halo of M31, which have characteristics between typical GCs and dwarf galaxies. Mackey et al. (2006) reported four extended, low-surface-brightness clusters in the halo of M31 based on *Hubble Space Telescope*/Advanced Camera for Surveys (ACS) imaging. These star clusters are structurally very different from typical M31 GCs. However, since they are old and metal-poor, they look like typical Milky Way GCs. Huxor (2007) found 40 new extended GCs in the halo of M31 out to $\sim$ 100 kpc from the galactic center based on INT and CFHT imaging. These extended star clusters in the M31 halo are very similar to the diffuse star clusters (DSCs) associated with early-type galaxies in the Virgo Cluster reported by Peng et al. (2006) based on the ACS Virgo Cluster survey. Indeed, evidence shows that DSCs are usually fainter than typical GCs. Later, Mackey et al. (2007) reported 10 outer-halo GCs in M31, at $\sim$15 kpc to 100 kpc from the galactic center, eight of which were newly discovered based on deep ACS imaging. The HGCs in their sample are very luminous and compact with low metallicity, which are quite different from their counterparts in our Galaxy. More recently, Ma et al. (2010) constrained the age, metallicity, reddening and distance modulus of B379, which is also an HGC of M31, based on the multicolor photometry.

In Fan et al. (2011) (hereafter Paper I) we observed 11 confirmed star clusters, most of which are located in the halo of M31, with the Optomechanics Research Inc. (OMR) spectrograph on the 2.16 m telescope at the Xinglong site of the National Astronomical Observatories, Chinese Academy of Sciences (NAOC), in the fall of 2010. We estimated the ages, metallicities, and α-elements with the Single Stellar Population (SSP) models as well as the radial velocities and found that most of the halo clusters are old and metal-poor, which indicates they were born in the early stage of the galaxy's formation history. In this paper, we will continue the study of the HGCs of M31 using the same instruments but with a larger sample. This allows us to better understand the properties of M31's outer halo. This paper is organized as follows. In Section 2 we describe how we selected our sample of M31 GCs and their spatial distribution. In Section 3, we report the spectroscopic observations with the 2.16 m telescope, how the data were reduced and how we measured and calibrated the radial velocities and Lick indices. Subsequently, in Section 4, we derive the ages, metallicities and α-elements with χ^2-minimization fitting. We also discuss our final results on the metallicity distribution in the M31 halo. Finally, we summarize our work and give our conclusions in Section 5.

2 SAMPLE SELECTION

The sources were selected from the updated Revised Bologna Catalog of M31 globular clusters and candidates (RBC v.4, available from *http://www.bo.astro.it/M31*; Galleti et al. 2004, 2006, 2007,

2009), which is the latest and most comprehensive M31 GC catalog so far. The catalog contains 2045 objects, including 663 confirmed star clusters, 604 cluster candidates, and 778 other objects that were previously thought to be GCs but later proved to be stars, asterisms, galaxies, or HII regions. Indeed, many of the halo clusters were from Mackey et al. (2007), who reported 10 GCs in the outer halo of M31 from their deep ACS images, of which eight were detected for the first time (for details see Sect. 1). In our work, the sample clusters were only selected from RBC v.4. We selected the confirmed and luminous clusters that were located far from the galaxy's center, where the effects of background contamination in the observations were minimized. Finally, there are eight bright confirmed clusters in our sample, all of which are located in the halo of the galaxy. These clusters lack observed spectroscopic data, especially for the metallicity measurements. Thus it is necessary to systematically observe the spectra of our sample clusters and carefully constrain the spectroscopic metallicities and ages.

The observational information of our sample GCs is listed in Table 1, which includes names, coordinates, projected radii in kpc, exposures and observation dates. All the coordinates (R.A. and Dec. in Cols. 2 and 3) and projected radii from the galactic center r_p (Col. 4) are from RBC v.4, which were calculated with the coordinate of M31's center, given by 00:42:44.31, +41:16:09.4 (Perrett et al. 2002), PA=38° and distance $d = 785$ kpc (McConnachie et al. 2005).

Table 1 Observations of Our Sample GCs

ID	R.A. (J2000) (h m s)	Dec. (J2000) (° ′ ″)	r_p (kpc)	Exposure (s)	Date
B289	00:34:20.882	+41:47:51.14	22.65	6000	2011/08/28
B290	00:34:20.947	+41:28:18.18	21.69	7200	2011/09/01
H11	00:37:28.028	+44:11:26.41	42.10	5400	2011/09/01
H18	00:43:36.030	+44:58:59.30	50.87	5400	2011/08/29
SK108A	00:47:14.240	+40:38:12.30	14.47	3600	2011/08/28
SK112A	00:48:15.870	+41:23:31.20	14.28	5400	2011/08/29
MGC1	00:50:42.459	+32:54:58.78	117.05	3600	2011/08/28
H25	00:59:34.560	+44:05:39.10	57.35	5400	2011/09/01

We show the spatial distribution of our eight sample halo GCs and all the confirmed GCs from RBC v.4 in Figure 1. The large ellipse is the M31 disk/halo boundary, as defined by Racine (1991). Note that all of our sample are located in the halo of M31, which can help us to compare properties of the galaxy's halo using an enlarged cluster sample with the results from Paper I.

3 OBSERVATIONS AND DATA REDUCTION

Our low-resolution spectroscopic observations were all taken with the 2.16 m optical telescope at the Xinglong Site, which belongs to the NAOC, from August 28th to September 1st, in 2011 (see Table 1). An OMR spectrograph and a PI 1340×400 CCD detector were used during this run with a dispersion of 200 Å mm^{-1}, 4.8 Å pixel^{-1}, and a 3.0″slit. The typical seeing there was $\sim 2.5''$. The spectra cover the wavelength range of $3500 - 8100$ Å at 4 Å resolution. All our spectra have S/N≥ 40.

In order to calibrate our data taken with the 2.16 m telescope onto the Lick system, we also observed 11 Lick standard stars (HR 6806, HR 6815, HR 7030, HR 7148, HR 7171, HR 7503, HR 7504, HR 7576, HR 7977, HR 8020, HR 8165) near our field, which are selected from a catalog of all 25 index measurements and coordinates for 460 stars (ref available from *http://astro.wsu.edu/worthey/html/system.html*; Worthey & Ottaviani 1997; Worthey et al. 1994). Most of these standard stars are luminous ($\sim 5 - 6$ in V band), so the exposure time was 20 s with the OMR system.
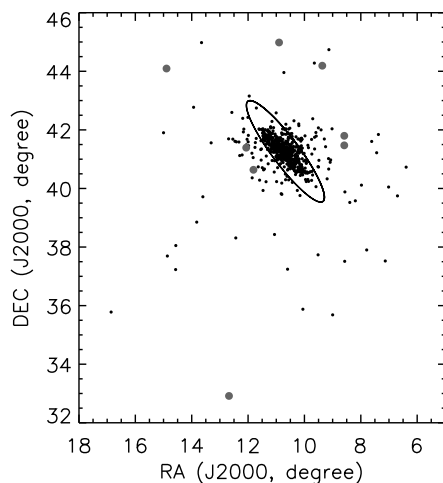
Fig. 1 Spatial distribution of M31 GCs. Our sample halo GCs are shown with filled circles and the confirmed GCs from RBC v.4 are marked with points. The large ellipse is the M31 disk/halo boundary as defined in Racine (1991).

The spectroscopic data were reduced following the standard procedures with NOAO Image Reduction and Analysis Facility (IRAF v.2.15) software package. First, the spectra have been bias and flat-field corrected, and cosmic-ray removal was performed. Then the wavelength calibrations were performed based on Helium/Argon lamps exposed at both the beginning and the end of the observations each night. Flux calibrations were performed based on observations of at least two of the KPNO standard spectral stars (Massey et al. 1988) each night. The atmospheric extinction was corrected with the mean extinction coefficient measurements of Xinglong derived from the Beijing-Arizona-Taiwan-Connecticut (BATC) multicolor sky survey (H. J. Yan 1995, priv. comm.).

Before the Lick indices were measured, the heliocentric radial velocities V_r were measured by comparing the absorption lines of our spectra with the templates in various radial velocities. The typical internal velocity errors in a single measurement were ~ 20 km s^{-1}. The estimated radial velocities V_r with the associated uncertainties (Col. 2) are listed in Table 2. The published radial velocities V_r (Col. 3) are also listed for comparison. The systematic difference between our observed velocity and the catalog's velocity is found to be 29 ± 39 km s^{-1} and the standard deviation of the differences between our observed velocity and the catalog's velocity is 78 km s^{-1} for the five pairs of radial velocities. It suggests that our measurements agree with those listed in RBC v.4 since the systematic difference between our measurements and the published values is not significant.

Figure 2 shows the radial velocity V_r (corrected for the systemic velocity of M31) as a function of the projected radii from the galaxy's center. The left panel is for all the confirmed GCs which have the measurements of radial velocity V_r and the right panel is for the HGCs, which refers to the GCs in the galaxy halo defined in Figure 1. It can be noted that the radial velocity distributions are basically symmetric for both the confirmed GC sample and the HGCs.

We plotted the radial velocities V_r versus the projected radii r_p in Figure 3, where the radial velocities have been corrected for the systemic velocity of galaxy M31, which is -300 ± 4 km s^{-1} (Perrett et al. 2002). The left panel is for all the confirmed clusters in RBC v.4 while the right panel is for the halo clusters which are defined in Figure 1. The points are the published measurements from RBC v.4 while the open triangles and filled circles with errors are the measurements in Paper I

Table 2 Radial velocities V_r of our sample GCs as well as the previous results.

| ID	Our work	RBC v.4
B289	-96.81 ± 47.27	-181 ± 30
B290	-488.73 ± 43.14	-381 ± 26
H11	-173.02 ± 39.63	
H18	-300.48 ± 79.65	
SK108A	-352.17 ± 19.18	-379 ± 38
SK112A	-342.68 ± 32.81	-252 ± 46
MGC1	-412.67 ± 17.13	-355 ± 2
H25	-256.49 ± 55.28	
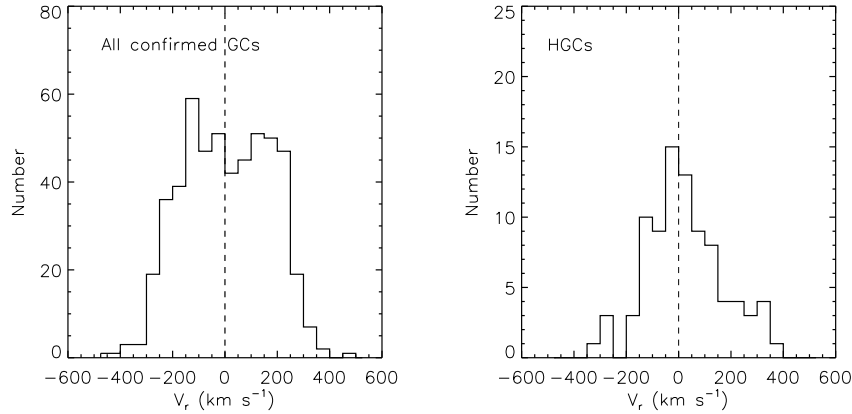
Fig. 2 Distributions of radial velocity V_r (corrected for the systemic velocity of M31). *Left*: all the confirmed GCs. *Right*: only the HGCs.

and those in our work, respectively. In the right panel, the symbols are the same as those in the left panel. We find that the dispersion of the velocity becomes smaller when the GCs are located further from the center of the galaxy with a larger projected radius r_p. It can be seen that the dispersion of the radial velocity becomes smaller when the projected radius r_p is larger.

Subsequently, all the spectra were shifted to zero radial velocity and smoothed to the wavelength dependent Lick resolution with a variable-width Gaussian kernel following the definition of Worthey & Ottaviani (1997), i.e. 11.5 Å at 4000 Å, 9.2 Å at 4400 Å, 8.4 Å at 4900 Å, 8.4 Å at 5400 Å, and 9.8 Å at 6000 Å. Indeed, we carefully measured all the 25 types of Lick indices by using the parameters and formulae from Worthey et al. (1994) and Worthey & Ottaviani (1997). The uncertainty of each index was estimated based on the analytic formulae (11)−(18) of Cardiel et al. (1998).

Equation (1) is the relation used in the linear fit for calibrating the raw measurements of our data taken with the 2.16 m telescope to the standard Lick index system. The 11 standard stars are utilized for the fitting (see Fig. 4) and the results are listed in Table 3.

$$\mathrm{EW}_{\mathrm{ref}} = a + b \cdot \mathrm{EW}_{\mathrm{raw}} . \tag{1}$$
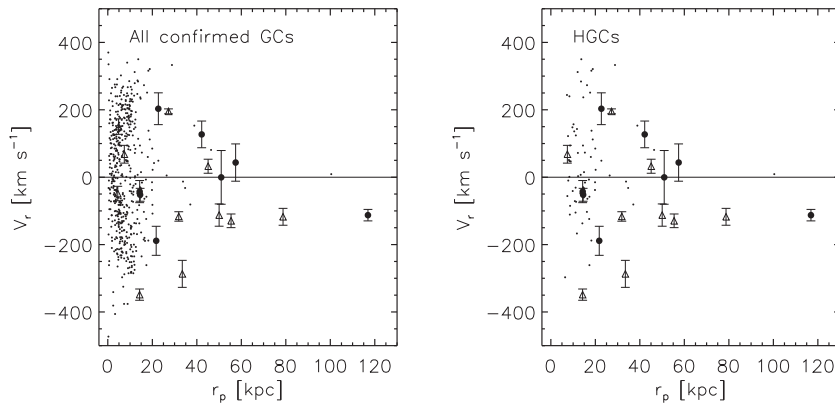
Fig. 3 Radial velocity V_r (corrected for the systemic velocity of M31) as a function of the projected radius. *Left*: all confirmed clusters and *Right*: the halo clusters. The filled circles with errors are the halo GCs from our sample while the points represent the velocities from the RBC v.4 catalog. The triangles denote the measurements from Paper I, and the associated bars are their errors.
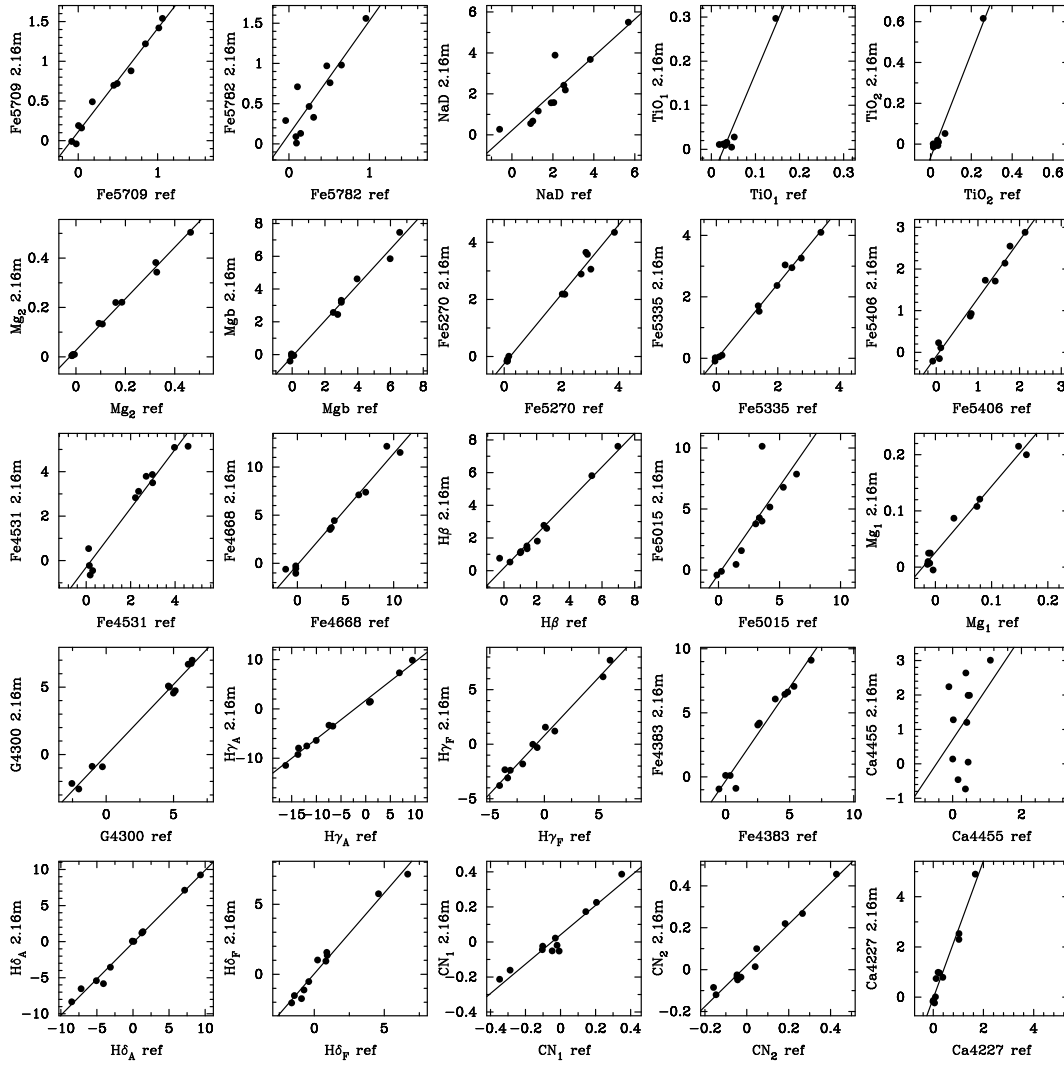
Table 3 The coefficients from the Linear Fit a and b in Eq. (3) for transformations of the data taken with the 2.16 m telescope to the Lick index system.

Index	a	b
Hδ_A (Å)	-0.15 ± 0.19	1.00 ± 0.04
Hδ_F (Å)	0.04 ± 0.15	1.15 ± 0.06
CN1 (mag)	0.04 ± 0.01	0.84 ± 0.07
CN2 (mag)	0.02 ± 0.01	0.98 ± 0.05
Ca4227 (Å)	-0.04 ± 0.14	2.73 ± 0.21
G4300 (Å)	-0.06 ± 0.19	1.05 ± 0.04
Hγ_A (Å)	1.73 ± 0.26	0.78 ± 0.03
Hγ_F (Å)	0.79 ± 0.16	1.07 ± 0.05
Fe4383 (Å)	-0.32 ± 0.36	1.46 ± 0.10
Ca4455 (Å)	0.71 ± 0.56	1.50 ± 1.21
Fe4531 (Å)	-0.30 ± 0.24	1.33 ± 0.09
Fe4668 (Å)	-0.16 ± 0.31	1.16 ± 0.06
Hβ (Å)	0.17 ± 0.16	1.03 ± 0.05
Fe5015 (Å)	-0.34 ± 1.07	1.44 ± 0.30
Mg1 (mag)	0.03 ± 0.01	1.18 ± 0.07
Mg2 (mag)	0.03 ± 0.01	1.04 ± 0.03
Mgb (Å)	-0.12 ± 0.15	1.09 ± 0.04
Fe5270 (Å)	-0.25 ± 0.11	1.21 ± 0.05
Fe5335 (Å)	-0.04 ± 0.06	1.23 ± 0.03
Fe5406 (Å)	-0.10 ± 0.08	1.39 ± 0.07
Fe5709 (Å)	0.11 ± 0.03	1.30 ± 0.06
Fe5782 (Å)	0.12 ± 0.10	1.41 ± 0.24
NaD (Å)	0.21 ± 0.36	0.91 ± 0.14
TiO1 (mag)	-0.07 ± 0.01	2.38 ± 0.19
TiO2 (mag)	-0.07 ± 0.01	2.56 ± 0.14

4 FITTING, ANALYSIS AND RESULTS

4.1 Model Description

Thomas et al. (2003) provided stellar population models that included Lick absorption line indices for various elemental-abundance ratios, covering ages from 1 to 15 Gyr and metallicities from 1/200

Fig. 4 Calibrations of index measurements from the 11 standard stars of 2.16 m raw spectra with those from references Worthey & Ottaviani (1997); Worthey et al. (1994). The coefficients from the linear fit of Eq. (3) have been derived to be used for calibrating our raw data to the Lick index system.

to $3.5\times$ solar abundance. These models are based on the standard models of Maraston (1998), with input stellar evolutionary tracks from Cassisi et al. (1997) and Bono et al. (1997) and a Salpeter (1955) stellar initial mass function. Thomas et al. (2004) improved the models by including higher-order Balmer absorption-line indices. They found that these Balmer indices are very sensitive to changes in the α/Fe ratio for supersolar metallicities. The latest stellar population model for Lick absorption-line indices (Thomas et al. 2011) is an improvement on Thomas et al. (2003) and Thomas et al. (2004). They were derived from the MILES stellar library, which provides a higher spectral resolution appropriate for MILES and SDSS spectroscopy, as well as flux calibration. The models cover ages from 0.1 to 15 Gyr, $[\mathrm{Z/H}]$ from -2.25 to 0.67 dex, and $[\alpha/\mathrm{Fe}]$ from -0.3 to 0.5 dex. In

Table 4 Metallicities [Fe/H] Derived from the Spectral Indices [MgFe], Mg2

Name	$[Fe/H]_{avg}$
B289	-1.83 ± 0.27
B290	-0.56 ± 0.63
H11	-0.49 ± 0.58
H18	-1.35 ± 0.65
SK108A	-2.35 ± 0.22
SK112A	-1.62 ± 0.43
MGC1	-2.06 ± 0.33
H25	-2.74 ± 0.47

Here we define $[Fe/H]_{avg} = \frac{[Fe/H]_{[MgFe]} + [Fe/H]_{Mg2}}{2}$.

our work, we fitted our absorption indices based on the models of Thomas et al. (2011), by using the two sets of stellar evolutionary tracks provided, i.e. Cassisi et al. (1997) and Padova.

4.2 Fits with Stellar Population Models and the Results

Similar to Sharina et al. (2006) and our Paper I, the χ^2−minimization routine was applied for fitting Lick indices with the SSP models to derive the physical parameters. Since we measured 25 different types of Lick line indices listed in Table 3, all indices were used for the fitting procedure. As Thomas et al. (2011) provided only 20 ages, six metallicities [Z/H], and four α-elements [α/Fe] for the SSP model, it is necessary to interpolate the original models to the higher-resolution models for our needs. We performed the cubic spline interpolations, using equal step lengths, to obtain a grid of 150 ages from 0.1 to 15 Gyr, 31 [Z/H] values from -2.25 to 0.67 dex, and 51 [α/Fe] values from -0.3 to 0.5 dex, which could make the fitted results smoother and more continuous. Worthey (1994); Galleti et al. (2009) pointed out the age-metallicity degeneracy remain almost the same for most of the spectral index measurements when the fraction changes as $\Delta \text{age}/\Delta Z = 3/2$. Therefore, it is necessary for us to constrain the metallicity with the metal-sensitive indices before the fits.

Fortunately, Galleti et al. (2009) provided two ways to directly measure the metallicity from the metal-sensitive spectral indices. One method is through combining the absorption line indices Mg and Fe, [MgFe], which is defined as $[MgFe] = \sqrt{Mgb \cdot \langle Fe \rangle}$, where $\langle Fe \rangle = (Fe5270 + Fe5335)/2$. Thus, the metallicity can be calculated from the formula below,

$$[Fe/H]_{[MgFe]} = -2.563 + 1.119[MgFe] - 0.106[MgFe]^2 \pm 0.15. \quad (2)$$

The second way to obtain the metallicity from Mg2 is by using a polynomial in the following,

$$[Fe/H]_{Mg2} = -2.276 + 13.053Mg2 - 16.462Mg2^2 \pm 0.15. \quad (3)$$

Finally we obtained values for $[Fe/H]_{avg}$ with associated uncertainties which are given in Table 4. This list gives an average of the metallicities derived from the metallicity Equations (2) and (3). The averaged metallicity $[Fe/H]_{avg}$ will be used to constrain the metallicity in the fits to break the age-metallicity trends/degeneracy. However, the Thomas et al. (2011) model only provided the metallicity parameters with [Z/H] and [α/Fe], thus we need to find a relationship between the iron abundance [Fe/H], total metallicity [Z/H] and α-element to iron ratio [α/Fe], so we can replace [Fe/H] with [Z/H] and [α/Fe] in the fitting procedure. In fact, Thomas et al. (2003) gave the relation in Equation (4).

$$[Z/H] = [Fe/H] + 0.94[\alpha/Fe]. \quad (4)$$

Here we would like to draw the reader's attention to the point that, although the metallicity [Fe/H] has been determined first, there are still many different ways to combine [Z/H] and [α/Fe] in the

parameter grid of the model. Therefore, we still need to simultaneously fit the age, [Z/H] and [α/Fe]. Here, we would like to constrain the metallicity in the fits for $|[\text{Fe/H}]_{\text{fit}} - [\text{Fe/H}]_{\text{avg}}| \leq 0.3$ dex, which is the typical metallicity uncertainty for the observations and it will make the fits more reasonable. As in Paper I, the physical parameters of ages, metallicities [Z/H], and [α/Fe] can be determined by comparing the interpolated stellar population models with the observed spectral indices by employing the χ^2-minimization method given by

$$\chi^2_{\text{min}} = \min \left[\sum_{i=1}^{25} \left(\frac{L_{\lambda_i}^{\text{obs}} - L_{\lambda_i}^{\text{model}}(\text{age}, [\text{Z/H}], [\alpha/\text{Fe}])}{\sigma_i} \right)^2 \right] , \qquad (5)$$

where $L_{\lambda_i}^{\text{model}}(\text{age}, [\text{Z/H}], [\alpha/\text{Fe}])$ is the ith Lick line index in the stellar population model for age, metallicity [Z/H] and [α/Fe], while $L_{\lambda_i}^{\text{obs}}$ represents the observed calibrated Lick absorption-line indices from our measurements. The errors estimated in our fitting are given as follows

$$\sigma_i^2 = \sigma_{\text{obs},i}^2 + \sigma_{\text{model},i}^2 . \qquad (6)$$

Here, $\sigma_{\text{obs},i}$ is the observational uncertainty while $\sigma_{\text{model},i}$ is the uncertainty associated with the models of Thomas et al. (2011). These two types of uncertainties have both been considered in our fitting procedure.

Table 5 lists the fitted ages, [Z/H] and [α/Fe] with different evolutionary tracks of Cassisi et al. (1997) and Padova. In addition, we calculated the [Fe/H]$_{\text{cassisi}}$ and [Fe/H]$_{\text{padova}}$ by applying Equation (4) to the fitted [Z/H] and [α/Fe]. In order to be consistent with Paper I, we adopted the metallicity [Fe/H]$_{\text{cassisi}}$ in the following statistics and analysis. From Table 5, we found that the ages, [Z/H] and the α-element [α/Fe] fitted from either Cassisi et al. (1997) or Padova tracks are consistent with each other. Additionally, it is worth noting that all of our sample halo GCs are older than 10 Gyr in both evolutionary tracks except B290 (5.5 to 5.8 Gyr), which is older than 2 Gyr and it should be identified as the "old" case in Caldwell et al. (2009). Thus, it indicates that these halo clusters formed at the early stage of the galaxy's formation process, which agrees well with previous findings.

Actually, Mackey et al. (2010) conclude that the metal abundance of MGC1, a star cluster listed in Tables 4 and 5, is about [Fe/H] $= -2.3$ and its age is 12.5 to 12.7 Gyr through the color-magnitude diagram fitting. The estimated age agrees well with our results but the metallicity is lower than our estimate [Fe/H]$_{\text{avg}} = -2.06 \pm 0.33$ in Table 4 or [Fe/H]$_{\text{cassis}} = -1.76 \pm 0.16$ in Table 5. Nevertheless, Alves-Brito et al. (2009) found that the metallicity [Fe/H] $= -1.37 \pm 0.15$ by combining the spectroscopic data and the photometric data, which is higher than our estimate. Hence, our result is just between the two former results, which suggests that our result is consistent with the previous conclusions.

Table 5 The χ^2-minimization Fitting Results Using Thomas et al. (2011) Models with Cassisi et al. (1997) and Padova Stellar Evolutionary Tracks

Name	Age (Gyr)	Cassisi [Z/H] (dex)	[α/Fe] (dex)	[Fe/H] (dex)	Age (Gyr)	Padova [Z/H] (dex)	[α/Fe] (dex)	[Fe/H] (dex)
B289	10.75 ± 4.15	-1.67 ± 0.23	0.34 ± 0.16	-2.09 ± 0.27	11.70 ± 2.80	-2.07 ± 0.18	-0.12 ± 0.18	-2.13 ± 0.25
B290	5.80 ± 2.40	-0.99 ± 0.05	-0.26 ± 0.05	-0.85 ± 0.07	5.50 ± 0.40	-1.33 ± 0.38	-0.26 ± 0.05	-0.85 ± 0.39
H11	13.75 ± 1.25	0.09 ± 0.32	0.08 ± 0.05	-0.19 ± 0.33	13.60 ± 0.20	-0.10 ± 0.24	0.00 ± 0.06	-0.21 ± 0.24
H18	13.45 ± 1.45	-0.47 ± 0.37	0.48 ± 0.02	-1.07 ± 0.37	13.60 ± 0.20	-0.50 ± 0.24	0.48 ± 0.02	-1.07 ± 0.24
SK108A	13.60 ± 0.30	-1.53 ± 0.18	0.28 ± 0.22	-2.09 ± 0.28	13.55 ± 0.45	-1.48 ± 0.23	0.27 ± 0.24	-2.09 ± 0.32
SK112A	11.10 ± 3.90	-1.33 ± 0.38	0.25 ± 0.25	-1.35 ± 0.45	11.70 ± 3.30	-1.51 ± 0.47	0.10 ± 0.40	-1.42 ± 0.61
MGC1	13.30 ± 0.80	-1.39 ± 0.14	0.42 ± 0.08	-1.76 ± 0.16	12.90 ± 1.30	-1.39 ± 0.14	0.42 ± 0.08	-1.76 ± 0.16
H25	13.60 ± 0.30	-1.98 ± 0.20	0.50 ± 0.00	-2.45 ± 0.20	13.50 ± 0.50	-2.03 ± 0.05	0.50 ± 0.00	-2.45 ± 0.05

### 4.3 Metallicity Properties of the Outer Halo

The metallicity gradients of the halo star clusters and stars are important to the formation and enrichment processes of their host galaxy. Basically, there are two possible scenarios for galaxy formation. One is that the halo stars and clusters should feature large-scale metallicity gradients if the enrichment timescale is shorter than the collapse time, which may be due to the galaxy's formation being a consequence of a monolithic, dissipative, and rapid collapse of a single massive, nearly spherical, spinning gas cloud (Eggen et al. 1962; Barmby et al. 2000). The other one is a chaotic scheme for early galactic evolution, when the loosely bound pre-enriched fragments merge with the protogalaxy during a very long period of time, in which case a more homogeneous metallicity distribution should develop (Searle & Zinn 1978). However, most galaxies are believed to have formed through a combination of these scenarios.

van den Bergh (1969); Huchra et al. (1982) showed that there is little to no evidence for a general radial metallicity gradient for GCs within a radius of 50 arcmin. However, studies including Huchra et al. (1991); Perrett et al. (2002); Fan et al. (2008) support the possible existence of a radial metallicity gradient for the metal-poor M31 GCs, although the slope is not very significant. Perrett et al. (2002) suggest that the gradients are -0.017 and -0.015 dex arcmin^{-1} for the full sample and inner metal-poor clusters respectively. More recently, Fan et al. (2008) found that the slope is -0.006 and -0.007 dex arcmin^{-1} for the metal-poor subsample and whole sample but the slope approaches zero for the metal-rich subsample. Nevertheless, all these studies are based on GCs that are located relatively close to the center of the galaxy, usually at projected radii of less than 100 arcmin. Recently, Huxor et al. (2011) investigated the metallicity gradient for 15 halo GCs to $r_{\mathrm{p}} = 117$ kpc with the metallicity derived from the CMD fittings (Mackey et al. 2006, 2007, 2010) and the authors found that the metallicity gradient becomes insignificant if one halo GC H14 is excluded from their figure 6. We found that our result is consistent with the previous findings of Huxor et al. (2011). In Paper I, we found the slope of the metallicity gradient is -0.018 ± 0.001 dex kpc^{-1} for the halo cluster sample extending to $r_{\mathrm{p}} \sim 117$ kpc from the galaxy's center. Further, the slope turns out to be -0.010 ± 0.002 dex kpc^{-1} if only considering the clusters $r_{\mathrm{p}} > 25$ kpc.

Since we have spectroscopic observations of eight more confirmed halo clusters, it is interesting to check if the metallicity distribution/spatial gradient would change with an enlarged halo cluster sample. For the new observed data, as we recalled in Section 4.2, only MGC1 has previous metallicity measurements from the literature, which are very different in different works and our measurement is just the median value. Thus, we adopted our measurement. Finally, we have a total metallicity sample of 391 entries.

Figure 5 shows the metallicity as a function of the projected radius from the galaxy's center for all outer GCs with spectroscopic metallicity at $r_{\mathrm{p}} > 25$ kpc from the galaxy's center. The slope of a linear fit is -0.005 ± 0.005 dex kpc^{-1}, which is marked with a solid black line. However, if the two star clusters with the highest metallicity, G001 and H11, are excluded, the slope turns out to be -0.002 ± 0.003 dex kpc^{-1}, which is shown with the red dashed line. Thus, both of these cases suggest that there is no metallicity gradient for the clusters in M31's outer halo when $r_{\mathrm{p}} > 25$ kpc, which agrees with the conclusion of Paper I. Therefore it seems that the "fragments merging" scenario dominated in the outer halo during a stage of the galaxy's formation process.

It should be noted that the metallicity gradient is fitted based on the data of our observations and the literature and the metallicities from different literature may not be the same. For instance, the metallicity of G001 is [Fe/H] $= -1.08 \pm 0.09$ in Huchra et al. (1991) but it is [Fe/H] $= -0.73 \pm 0.15$ in Galleti et al. (2009). Thus we wonder how the slope would change when the data change. We simulated ten sets of random data from $\sigma = -0.5$ to 0.5 and added them to the metallicities that we used in Figure 5 and then separately refit the slopes again ten times. The results are shown in Table 6. It shows that the slope does not change significantly when the simulated errors were added, suggesting that the slope is stable even across data from different measurements.
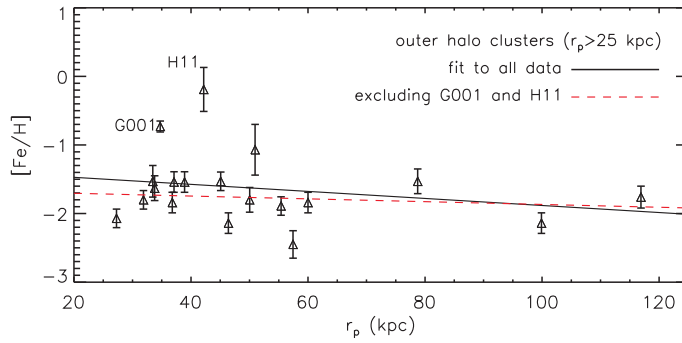
Fig. 5 Metallicities [Fe/H] versus projected radii for the outer halo GCs at $r_p > 25$ kpc from the center of the galaxy. The slope of the linear fitting is -0.005 ± 0.005 dex kpc^{-1} (*black solid line*). However, if the two GCs with the highest metallicity, G001 and H11, are excluded, the slope turns out to be -0.002 ± 0.003 dex kpc^{-1} (*dashed line*).
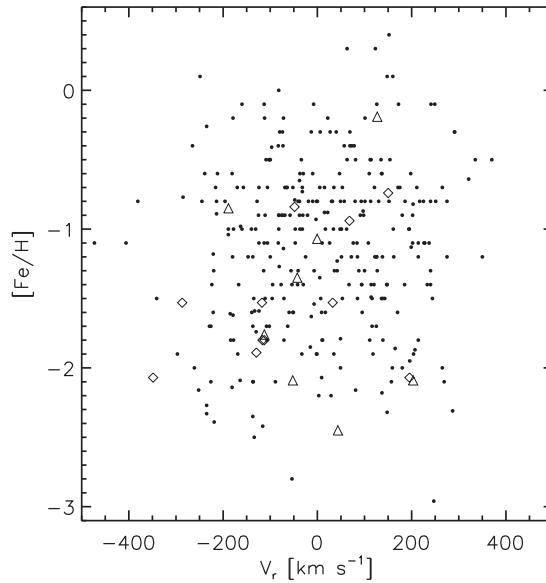

Fig. 6 Metallicity [Fe/H] versus radial velocity V_r (corrected for the systemic velocity of M31) for all the GCs with spectroscopic metallicities and radial velocity. The small points are from the literature; the squares are from Paper I; the triangles are our measurements.

Figure 6 shows the relationship between the metallicities and the radial velocities V_r which have been corrected for the systemic velocity of the galaxy M31. The spectroscopic metallicities are from the literature (Huchra et al. 1991; Barmby et al. 2000; Perrett et al. 2002; Galleti et al. 2009; Caldwell et al. 2011) and Paper I as well as from this work and the radial velocities V_r are from the RBC v.4, Paper I and this work. It seems that there is no relationship between the metallicities and the radial velocities V_r.

**Table 6** Slopes of Metallicity Gradient by Adding the
Random Errors to the Data

No.	k_{all}	$k_{<-1}$
1	-0.013 ± 0.010	-0.013 ± 0.011
2	-0.003 ± 0.010	0.000 ± 0.014
3	-0.011 ± 0.012	-0.008 ± 0.012
4	-0.009 ± 0.009	0.000 ± 0.012
5	-0.003 ± 0.013	-0.036 ± 0.021
6	-0.002 ± 0.012	0.004 ± 0.022
7	-0.004 ± 0.013	-0.002 ± 0.022
8	-0.009 ± 0.012	0.009 ± 0.015
9	-0.005 ± 0.010	-0.008 ± 0.017
10	-0.013 ± 0.011	0.003 ± 0.008
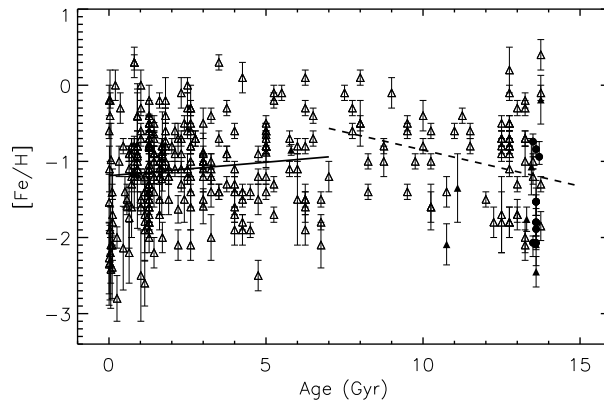
Fig. 7 Metallicity $[\mathrm{Fe/H}]$ versus age for all the clusters with spectroscopic metallicity and age estimates. The open triangles are the data from the literature; the filled circles are the data from Paper I; the filled triangles are the data from this work. The solid line represents the linear fit of GCs younger than 7 Gyr while the dashed line is the fit for the GCs older than 7 Gyr.

Figure 7 shows the metallicities versus ages of the GCs. The metallicities are from the literature (Huchra et al. 1991; Barmby et al. 2000; Perrett et al. 2002; Galleti et al. 2009; Caldwell et al. 2011) and Paper I as well as from this work and the ages are from Fan et al. (2010), Paper I and this work. We wanted to see if there was a relationship between the ages and metallicities of these GCs. We found that the relationships are different for the GC populations with different ages. The slope of the GCs younger than 7 Gyr is $k = 0.035 \pm 0.021$ but the slope of the GCs older than 7 Gyr is $k = -0.095 \pm 0.034$, which is at the $\sim 3\sigma$ significance level. It suggests that for the GCs younger than 7 Gyr, there is no relationship between age and metallicity but for the clusters older than 7 Gyr, it seems that the older GCs are more metal-poor (lower metallicity) and the younger GCs are more metal-rich (higher metallicity).

Previously, many astronomers found a significant bimodal case in the distribution of metallicity in M31 GCs by applying the mixture-model method of the KMM test (Ashman et al. 1994). Ashman & Bird (1993); Barmby et al. (2000); Perrett et al. (2002) found the proportion of the metal-poor to metal-rich group is $\sim$2:1 to $\sim$3:1 with the peak positions of $[\mathrm{Fe/H}] \approx -1.5$ and -0.6, respectively. Fan et al. (2008) examined the bimodality of this metallicity distribution with a larger sample and the
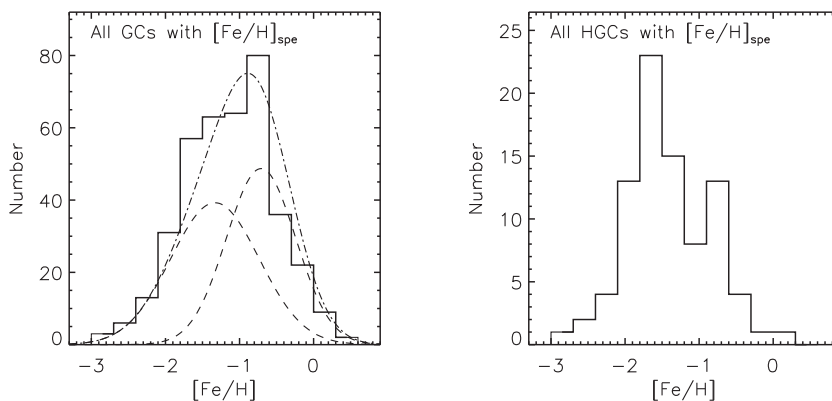
Fig. 8 Metallicity distributions with a bin size of 0.3 dex. *Left*: all the GCs with spectroscopic metallicities. The mixture-model KMM test was applied to divide them into two groups. *Right*: all the HGCs with spectroscopic metallicities.

authors found that the proportion is $\sim 1.5{:}1$ and the peak positions are $[\mathrm{Fe/H}] \sim -1.7$ and ~ -0.7, respectively. However, the recent work of Caldwell et al. (2011) suggests that there is no significant bimodality or trimodality for the metallicity distribution in a sample of 322 M31 GCs, most of which have spectroscopic metallicity with high S/N ratios. Since we have new observational data and a larger spectroscopic data sample, we are able to re-examine the bimodality of the metallicity distributions of M31 GCs.

Figure 8 shows the metallicity distributions of the GCs and the HGCs. In the left panel, the sample includes all the GCs which have spectroscopic metallicity from the literature (Huchra et al. 1991; Barmby et al. 2000; Perrett et al. 2002; Galleti et al. 2009; Caldwell et al. 2011) and Paper I as well as this work. In total, there are 386 GCs with spectroscopic metallicity in the distribution. We applied the mixture-model KMM algorithm to the dataset and it returned a negative result for bimodality with p-value $= 0.369$, which means that a bimodal distribution is preferred over a unimodal one at a 63.1% confidence level, less than what is needed to believe that bimodality is present. The numbers of the metal-poor group and the metal-rich group are $N1 = 196$ and $N2 = 190$, respectively and the mean values of the two groups are $[\mathrm{Fe/H}]_1 = -1.43$ ($\sigma_1^2 = 0.327$) and $[\mathrm{Fe/H}]_2 = -0.73$ ($\sigma_2^2 = 0.215$), respectively. As we can see from the plot, the proportion of the metal-poor to metal-rich group is $\sim 1 : 1$, which is lower than the published results. The reason why the bimodal case becomes more insignificant with a larger sample size may be that more intermediate metallicity GCs (which are between the two metallicity peaks) have been discovered and those intermediate metallicity GCs cause the distribution to be unlike a bimodal or trimodal distribution. Therefore, the previous works found that the metallicity distributions of M31 GCs is like that of the Milky Way and more recent works with more data show that they are less similar to each other, which may indicate that the formation processes of the two GC systems were markedly different. The right panel shows the metallicity distribution of the HGCs and obviously the metal-poor GCs dominate in the distribution.

As the M31 GCs have been divided into two different groups by the KMM test in the metallicity distribution of Figure 8, we would like to examine the spatial distributions of the two groups with different metallicities.

Figure 9 plots the spatial distributions of the metal-rich and metal-poor groups. Note that the metal-poor group appears to occupy a more extended halo and shows a wide spatial distribution, but the metal-rich group is more centrally concentrated, which is consistent with the conclusions of Perrett et al. (2002); Fan et al. (2008).
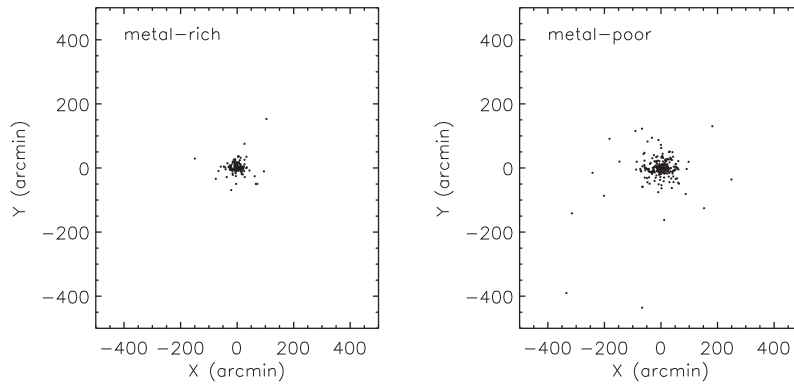
Fig. 9 Spatial distributions of HGCs with different metallicities. *Left*: metal-rich GCs; *Right*: metal-poor GCs. Members of the two groups were identified by the KMM test of Fig. 8.
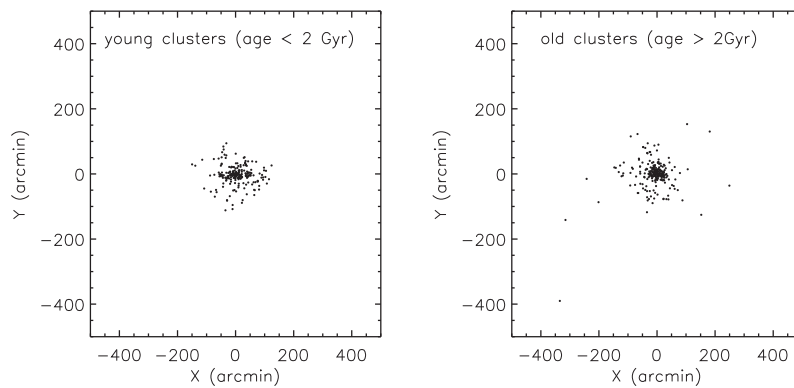
Fig. 10 Spatial distributions of HGCs with young and old populations. *Left*: young clusters with age < 2 Gyr; *Right*: old clusters with age > 2 Gyr.

Since we have the age estimates of the halo GCs in M31, we are curious about whether the spatial distributions of the young and old populations are the same or not. Here we used the definition of "old population" for age > 2 Gyr and "young population" for age < 2 Gyr as was done in Caldwell et al. (2009). For the purpose of enlarging our sample size, the age estimates for M31 GCs in Fan et al. (2010) and Paper I are also merged into our sample.

Figure 10 plots the spatial distributions of the young and old populations, respectively. It is obvious that the young population is more centrally concentrated and it traces the disk shape of the galaxy well. However, the spatial distribution of the old population is more dispersed and it seems that the members of that population do not trace the disk shape of the galaxy.

5 SUMMARY AND CONCLUSIONS

This is the second paper in our series of works on M31 halo globular clusters. In Paper I, we mainly focus on the fitting method and the metallicity gradient for the M31 GC sample. In this paper,

we focus on the dynamics, metallicity and age, and their distributions as well as the relationships between these parameters.

We selected eight more bright confirmed GCs in the halo of M31 from RBC v.4 and observed them with the OMR spectrograph on the 2.16 m telescope at the Xinglong site of NAOC in the fall of 2011. These star clusters are located in the halo of the galaxy at a projected radius of ~ 14 to ~ 117 kpc from the galactic center, where the sky background is dark so that they can be observed with high signal-to-noise ratios.

For all our sample clusters, we measured all 25 Lick absorption-line indices (see the definitions in Worthey et al. 1994; Worthey & Ottaviani 1997) and fitted the radial velocities. We found that distributions of the confirmed GCs and the halo GCs are basically symmetric with respect to the systematic velocity of the galaxy.

Similar to Sharina et al. (2006) and our Paper I, we applied the χ^2-minimization method to fit the Lick absorption line indices with the updated Thomas et al. (2011) stellar population model in two stellar evolutionary tracks of Cassisi and Padova, separately. The fitting results show that most of our sample clusters are older than 10 Gyr except B290~ 5.5 Gyr and most of them are metal-poor with metallicity $[\text{Fe/H}] < -1$ dex except H11 and H18, suggesting that these halo star clusters were born at an early stage of the galaxy's formation.

Again, we would like to study the metallicity gradient of the halo GCs by combining more spectroscopic metallicity values from this work, Paper I and the literature. We only considered outer halo clusters with $r_{\text{p}} > 25$ kpc and the fitted slope is -0.005 ± 0.005 dex kpc^{-1}. However, if two metal-rich clusters G001 and H11 that are outliers are excluded, the slope becomes -0.002 ± 0.003 dex kpc^{-1}, which does not show a significant change. Furthermore, in order to eliminate the effect of errors from different observations, we added the random errors from $\sigma = -0.5$ to 0.5 to the data and refitted the slope ten times. The result shows that the simulated errors do not affect the slope much. Thus it seems that the metallicity gradient for clusters in M31's outer halo does not exist, which is consistent with previous findings in (Huxor et al. 2011) and Paper I. This result may imply that the "fragments merging" scenario dominated in the outer halo of the galaxy beyond 25 kpc from the center during the early stage of the galaxy's formation process.

We do not find a relationship between metallicity and radial velocity for the sample of M31 GCs. It seems that the metallicity is not a function of age for the GCs with age < 7 Gyr, but for the old GCs with age > 7 Gyr there seems to be a trend that the older ones have lower metallicity. This conclusion is similar to that of Fan et al. (2006), who found a possible general trend of the age-metallicity relation with a large scatter. In addition, we plot metallicity distributions with the largest sample size of M31 GCs so far and it shows the bimodality is not significant compared to the previous work. This is also found by Caldwell et al. (2011), who used the newly observed spectroscopic data. We also find that the number of metal-poor and metal-rich groups becomes comparable but the previous works show that the number of metal-poor groups is more than that of the metal-rich ones. This may be due to the fact that many intermediate metallicity values of Caldwell et al. (2011) have been merged into our sample for our statistics. The spatial distribution shows that the metal-rich group is more centrally concentrated but the metal-poor group occupies a more extended halo; the young population is centrally concentrated while the old population is more spatially extended to the outer halo. This is easy to understand as the old GCs are usually metal-poor, especially for the halo GCs of M31.

References

Alves-Brito, A., Forbes, D. A., Mendel, J. T., Hau, G. K. T., & Murphy, M. T. 2009, MNRAS, 395, L34

Ashman, K. M., & Bird, C. M. 1993, AJ, 106, 2281

Ashman, K. M., Bird, C. M., & Zepf, S. E. 1994, AJ, 108, 2348

Barmby, P., Huchra, J. P., Brodie, J. P., et al. 2000, AJ, 119, 727

Barmby, P., & Huchra, J. P. 2001, AJ, 122, 2458

Bono, G., Caputo, F., Cassisi, S., Castellani, V., & Marconi, M. 1997, ApJ, 489, 822

Caldwell, N., Harding, P., Morrison, H., et al. 2009, AJ, 137, 94

Caldwell, N., Schiavon, R., Morrison, H., Rose, J. A., & Harding, P. 2011, AJ, 141, 61

Cardiel, N., Gorgas, J., Cenarro, J., & Gonzalez, J. J. 1998, A&AS, 127, 597

Cassisi, S., Castellani, M., & Castellani, V. 1997, A&A, 317, 108

Eggen, O. J., Lynden-Bell, D., & Sandage, A. R. 1962, ApJ, 136, 748

Fan, Z., Ma, J., de Grijs, R., Yang, Y., & Zhou, X. 2006, MNRAS, 371, 1648

Fan, Z., Ma, J., de Grijs, R., & Zhou, X. 2008, MNRAS, 385, 1973

Fan, Z., de Grijs, R., & Zhou, X. 2010, ApJ, 725, 200

Fan, Z., Huang, Y.-F., Li, J.-Z., et al. 2011, RAA (Research in Astronomy and Astrophysics), 11, 1298 (Paper I)

Galleti, S., Federici, L., Bellazzini, M., Fusi Pecci, F., & Macrina, S. 2004, A&A, 416, 917

Galleti, S., Federici, L., Bellazzini, M., Buzzoni, A., & Fusi Pecci, F. 2006, A&A, 456, 985

Galleti, S., Bellazzini, M., Federici, L., Buzzoni, A., & Fusi Pecci, F. 2007, A&A, 471, 127

Galleti, S., Bellazzini, M., Buzzoni, A., Federici, L., & Fusi Pecci, F. 2009, A&A, 508, 1285

Huchra, J., Stauffer, J., & van Speybroeck, L. 1982, ApJ, 259, L57

Huchra, J. P., Brodie, J. P., & Kent, S. M. 1991, ApJ, 370, 495

Huxor, A. 2006, Ph.D. Thesis, Univ. of Hertfordshire, UK

Huxor, A., Tanvir, N. R., Irwin, M., et al. 2004, in Astronomical Society of the Pacific Conference Series 327, Satellites and Tidal Streams, eds. F. Prada, D. Martinez Delgado, & T. J. Mahoney (San Francisco: ASP), 118

Huxor, A. P., Tanvir, N. R., Irwin, M. J., et al. 2005, MNRAS, 360, 1007

Huxor, A. P., Ferguson, A. M. N., Tanvir, N. R., et al. 2011, MNRAS, 414, 770

Ma, J., Wu, Z., Wang, S., et al. 2010, PASP, 122, 1164

Mackey, A. D., Huxor, A., Ferguson, A. M. N., et al. 2006, ApJ, 653, L105

Mackey, A. D., Huxor, A., Ferguson, A. M. N., et al. 2007, ApJ, 655, L85

Mackey, A. D., Ferguson, A. M. N., Irwin, M. J., et al. 2010, MNRAS, 401, 533

Maraston, C. 1998, MNRAS, 300, 872

Massey, P., Strobel, K., Barnes, J. V., & Anderson, E. 1988, ApJ, 328, 315

McConnachie, A. W., Irwin, M. J., Ferguson, A. M. N., et al. 2005, MNRAS, 356, 979

Peng, E. W., Côté, P., Jordán, A., et al. 2006, ApJ, 639, 838

Perina, S., Cohen, J. G., Barmby, P., et al. 2010, A&A, 511, A23

Perrett, K. M., Bridges, T. J., Hanes, D. A., et al. 2002, AJ, 123, 2490

Racine, R. 1991, AJ, 101, 865

Salpeter, E. E. 1955, ApJ, 121, 161

Searle, L., & Zinn, R. 1978, ApJ, 225, 357

Sharina, M. E., Afanasiev, V. L., & Puzia, T. H. 2006, MNRAS, 372, 1259

Thomas, D., Maraston, C., & Bender, R. 2003, MNRAS, 339, 897

Thomas, D., Maraston, C., & Korn, A. 2004, MNRAS, 351, L19

Thomas, D., Maraston, C., & Johansson, J. 2011, MNRAS, 412, 2183

van den Bergh, S. 1969, ApJS, 19, 145

Worthey, G. 1994, ApJS, 95, 107

Worthey, G., Faber, S. M., Gonzalez, J. J., & Burstein, D. 1994, ApJS, 94, 687

Worthey, G., & Ottaviani, D. L. 1997, ApJS, 111, 377